Journal of Environmental Management 380 (2025) 124741

Contents lists available at ScienceDirect

Journal of Environmental Management

journal homepage: www.elsevier.com/locate/jenvman

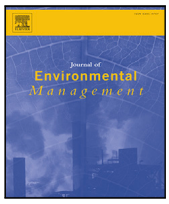

Research article

Non-radiative effects dominate the local surface temperature response to land-cover change—Insights from a semi-empirical model

Lorenz Hänchen [a,*], Benjamin Quesada [b], Almut Arneth [c]

[a] Department of Ecology, University of Innsbruck, Sternwartestrasse 15, Innsbruck, 6020, Austria
[b] Earth System Science Program, Faculty of Natural Sciences, Interactions Climate-Ecosystems (ICE) Research Group, Universidad del Rosario, Carrera 26, 63b-48, Bogotá, DC 111221, Colombia
[c] Institute of Meteorology and Climate Research, Atmospheric Environmental Research, Karlsruhe Institute of Technology, Kreuzeckbahnstraße 19, Garmisch-Partenkirchen, 82467, Germany

ARTICLE INFO

Keywords:
LCC
Biophysical effects
Surface temperature change
Climate policies

ABSTRACT

Land-cover change (LCC) is an important driver of climate change through carbon emissions (biochemical effects), but also through changes in the surface energy balance (biophysical effects). Quantifying magnitude and sign of surface temperature responses to biophysical effects is still challenging and under debate. We develop a new semi-empirical model based on a linearized surface energy balance for biophysical and an empirical model for the biochemical responses to LCC. Neglecting indirect effects, we find average global direct biophysical and biochemical warmings in response to a stylized deforestation scenario (1.22 K and 0.50 K) and historical LCC (0.42 K and 0.15 K), whereas an afforestation experiment leads to cooling (−1.95 K and −0.96 K). Our results underline the non-negligible impact of biophysical effects, especially non-radiative effects, and stress the importance of including these in the assessment of climate change mitigation and adaptation policies.

1. Introduction

Land-cover changes (LCC) are chiefly associated with the replacement of natural vegetation by vegetation types useful to humans, such as different types of crops, grassland for livestock, infrastructure and settlements, but include also abandoned agricultural areas in which natural vegetation regrows. Forests and natural ecosystems more broadly are beneficial to humankind beyond their economic value, such as regulation of the hydrological cycle, protection from erosion, being habitats for many species, and modulating the climate. By today, forests cover approximately 30% of the global land surface (Bonan, 2008). In recent decades, deforestation has occurred primarily in the tropics (Hansen et al., 2013), driven by large-scale expansion of agriculture and pastures (Gibbs et al., 2010). In temperate and boreal regions, the forest area has expanded since the second half of the twentieth century after land abandonment but also due to large-scale reforestation and afforestation activities (Li et al., 2018; Gerlein-Safdi et al., 2020; Nabuurs et al., 2007). These land-cover changes reflect also growing global trade, which increasingly spatially separates consumption and production of food, livestock and resources (Lambin and Meyfroidt, 2011; Fuchs et al., 2020).

LCC effects on climate can be classified into two categories. First, changes in the fluxes of gases (i.e. greenhouse gases like CO_2, N_2O, CH_4) caused by changes in land use and/or land-cover, here referred to as "biochemical effects". Second, impacts on the surface energy balance in response to changes in surface properties like albedo, surface roughness and evapotranspiration, referred here as "biophysical effects" (e.g. Lawrence et al., 2022; Conte et al., 2019; Alkama and Cescatti, 2016; Lee et al., 2011). Following deforestation, for example, the biochemical effects on surface temperature are mainly due to the release of carbon, with the overall magnitude depending on the type of land-cover transition and the intensity of land-use of the replacement agricultural ecosystem (Kirschbaum et al., 2013).

Since CO_2, N_2O, CH_4 are well-mixed greenhouse gases with atmospheric lifetimes from years to decades (CH_4) to centuries (CO_2, N_2O), biochemical effects have global impacts that accumulate over time. Biophysical effects on the other hand are more immediate and local. Neglecting potential feedbacks, deforestation associated with an increase in albedo results in local cooling through a negative radiative forcing. For boreal regions, this effect is strongly enhanced because forests can effectively mask snow (Bathiany et al., 2010), which should be considered, e.g., by critically reviewing boreal afforestation efforts as part of climate mitigation strategies (e.g. Bonan et al., 1992; Betts, 2011). The climatic impact of the other two direct biophysical effects,

* Corresponding author.
E-mail address: lorenz.haenchen@uibk.ac.at (L. Hänchen).

https://doi.org/10.1016/j.jenvman.2025.124741
Received 13 September 2024; Received in revised form 17 February 2025; Accepted 25 February 2025
Available online 13 March 2025

which are changes in roughness and evapotranspiration (Davin and de Noblet-Ducoudre, 2010), cannot solely be expressed via radiative forcing alone. There is however a noticeable effect on surface temperature, because changes in evapotranspiration and roughness alter the energy exchange between the surface and the atmosphere through turbulent heat fluxes (sensible (H) and latent (λE)) (Davin et al., 2007; Bala et al., 2007; Boisier et al., 2012; Bright et al., 2017; Panwar et al., 2020; Conte et al., 2019).

In addition, the biophysical effects can cause indirect and remote effects, among which are changes in cloud cover or large-scale atmospheric circulations through changes in the partitioning of sensible and latent heat flux or sea-ice/sea-surface-temperature feedbacks. The magnitude of remote effects depends on the areal extent and location of the LCC and, in idealized experiments, they tend to dominate over the local effects (Davin and de Noblet-Ducoudre, 2010; Winckler et al., 2019a; Devaraju et al., 2018; Quesada et al., 2017; Duveiller et al., 2018). The biophysical effects following LCC have recently been more systematically included in climate change assessments such as the IPCC (Myhre et al., 2013; Forster et al., 2021), but in climate policy measures that aim to achieve the Paris Agreement such as land-based mitigation measures in nationally determined contributions (NDC) they are still neglected (Perugini et al., 2017).

LCC is one of the key drivers of climate change but to date, the quantification of its biophysical vs. biochemical impacts still lacks consensus and there is a need of understanding the underlying processes of LCC on climate (Arneth et al., 2017; Houghton et al., 2012; Le Quéré et al., 2016; Pielke et al., 2011). Reliably evaluating these underlying processes presents significant challenges. Observation-based studies often rely on a space-for-time approach, which assumes that temperature differences between two land covers with the same background climate reflect local LCC (Duveiller et al., 2018). However, such approaches do not account for remote effects of deforested pixels, trends in climate partly driven by land-cover changes, or variations in hydroclimatic dynamics between adjacent pixels that violate the assumption of a uniform background climate. Taken together, these limitations lead to a warming bias of deforestation impacts compared to modeling approaches (Quesada et al., 2017; Perugini et al., 2017; Jia et al., 2019; Sy and Quesada, 2020).

Simulations with Earth System Models (ESMs), on the other hand, can provide important insights, but are computationally expensive and are often based on lengthy model intercomparisons as an approach to identify robust messages (e.g. De Noblet-Ducoudré et al., 2012; Brovkin et al., 2013; Boysen et al., 2020). Additionally, the lack of spatial resolution and the focus of most studies on idealized scenarios, inducing dominant feedback mechanisms (Jia et al., 2019; Perugini et al., 2017), prohibit the assessment of realistic local impacts of LCC, at least on the global scale (Lawrence et al., 2022). On smaller spatial scales, regional climate models (RCMs) have partially addressed these challenges, particularly through stylized afforestation scenarios, such as those explored in the Land-Use and Climate Across Scales (LUCAS) project (e.g. Davin et al., 2020; Asselin et al., 2022). Additionally, RCMs have been applied to investigate climate responses to observed LCC, for example for Europe and Asia (e.g. Huang et al., 2020; Cao et al., 2021). Nath et al. (2023) have recently introduced a novel framework to overcome the computational limitations by using an emulator approach based on multiple ESM outputs and observations. Despite these significant efforts, isolating and mechanistically attributing the specific biophysical and biochemical contributions to surface temperature changes remains challenging.

Semi-empirical approaches offer a middle ground by combining the computational efficiency of observation-based methods with being based on physical principles that allow studying individual mechanisms and testing a wide range of scenarios. To our knowledge, such approaches with the exception of the previously mentioned emulator by Nath et al. (2023), have so far not been widely explored in the context of LCC. As the computational cost of ESMs are not only high but also their complexity continuously increases, while at the same time the need for suitable climate change mitigation and adaptation strategies increases, there is a demand for efficient strategies to understand a wide range of LCC scenarios.

The overarching aim of this study is thus to provide a fast and easy-to-use tool which (i) finds the right balance between providing reasonable estimates of LCC mechanisms impacts on surface temperature while remaining sufficiently simple; (ii) bridges the gap between modeling and observation-based studies; (iii) disentangles the relative contribution of each biophysical mechanism and their spatial dependence.

2. Materials and methods

2.1. Model equations

To calculate the alteration of surface temperature by changes in surface properties through LCC, we make use of an idealized linearization of the surface energy balance equation, similar to previous studies (e.g., Lee et al. (2011), Chen and Dirmeyer (2016), Juang et al. (2007), Devaraju et al. (2018), Luyssaert et al. (2014)). In all studies, surface temperature is derived from the long-wave emission term ignoring non-linear interactions which suggests a potential underestimation of absolute changes (Zhao and Jackson, 2014). There seems to be a different conception of the impacts of LCC on both air and surface temperature between different studies, which hampers interpretation of results, especially on a policy level. Despite other differences, most of the studies that employ data from pairwise observation sites attribute air temperature differences between pairwise sites to LCC (e.g. Chen and Dirmeyer, 2016; Juang et al., 2007; Luyssaert et al., 2014) which contributes to the assessment of surface temperature change. In contrast, the formulation of Lee et al. (2011) assumes that the air temperature is identical at the blending height over the pairwise sites, which introduces a counteracting mechanism to the biophysical mechanisms. Several studies pointed out mechanistic differences between surface and air temperature responses (e.g. Baldocchi and Ma, 2013; Panwar et al., 2020) and contrasting different sensitivities to LCC (e.g. Winckler et al., 2019b; Novick and Katul, 2020). Chen and Dirmeyer (2016) extended the methodology of Lee et al. (2011) by adding a term representing the interaction between air and surface temperature and interpreting it as an indirect effect that includes background atmospheric change. As a change in air temperature was also observed after local LCC (e.g. Zhang et al., 2014; Alkama and Cescatti, 2016), we argue that both assuming no change in air temperature or attributing all change to remote/indirect effects are unlikely. However, the term representing the difference between the changes in air and surface temperature is relatively small compared to the other terms in the linearized surface energy balance. We acknowledge that on seasonal (e.g. Winckler et al., 2019b) or diurnal scales (e.g. Panwar et al., 2020; Novick and Katul, 2020) this effect can be relevant but magnitudes are smaller on annual scale, especially in comparison to assuming air temperature changes to be absent. Actual indirect effects (i.e. changes in incoming short- and long-wave radiation) and other effects with minor magnitude (i.e. change in ground heat flux and air density) are thus neglected compared to the other terms.

Here, we estimate the biophysical effects for a given LCC as follows.

$$\Delta T_{s(bph)} \approx \frac{\overbrace{-\Delta\alpha S\downarrow - \Delta\epsilon\sigma T_s^4}^{(1)} + \overbrace{R_n^* \frac{\Delta r_a}{r_a}}^{(2)} + \overbrace{\frac{R_n^* \Delta\beta}{(1+\frac{1}{\beta})\beta^2}}^{(3)}}{4\epsilon\sigma T_s^3} \quad (1)$$

$\Delta T_{s(bph)}$ represents the change in surface temperature due to biophysical effects, $\Delta\alpha$ is the change in surface albedo, $S\downarrow$ the incoming

shortwave radiation, $\Delta\epsilon$ the change in surface emissivity, σT_s^4 represents the longwave radiation emitted by the surface, as described by the Stefan–Boltzmann law, R_n^* represents the net radiation at the surface, r_a represents the aerodynamic resistance and β the Bowen Ratio which is the fraction of turbulent sensible and latent heat. For the detailed linearization and its rationale, consult Section 2 of the Supplementary Material.

With Eq. (1), the biophysical effects on surface temperature are estimated for each of the contributions individually. (1) refers to the albedo effect ($\Delta T_{s(\alpha)}$). It is proportional to the amount of incident radiation (higher in the tropics, smaller in boreal latitudes, and increasing with elevation). In general, deforestation tends to increase albedo (negative $\Delta\alpha$) with stronger impacts in areas where seasonal snow cover is present due to the snow-masking effect of forests. Following that, ΔT_s is negatively correlated to $\Delta\alpha$ all other parameters being equal. The change in surface emissivity ($\Delta\epsilon$) is negatively correlated with the albedo change ($\Delta\alpha$) and dampens its effect. We parameterize surface emissivity by using an assumption of $\epsilon = 0.99 - 0.16\ \alpha$ put forward by Juang et al. (2007). The second term (2) refers to the change in aerodynamic resistance ($\Delta T_{s(r_a)}$). When LCC occurs, r_a is primarily altered by the change in surface roughness length (z_0) and friction velocity (u^*) and affects the efficiency of the surface to exchange turbulent heat with the atmosphere. Term (3) calculates the change in the energy partition between sensible (H) and latent heat flux (λE) using the Bowen Ratio ($\beta = H/\lambda E$) and its effect on surface temperature ($\Delta T_{s(\beta)}$). As $\Delta\beta$ scales with β^2 the effect of LCC will be larger where the background Bowen ratio is smaller and vice versa. Generally, Eq. (1) is only valid for longer time scales, since the surface energy balance has to be in a steady state, which means that transient ground heat storage is neglected.

To compare the direct impacts of the biophysical effects with the biochemical impacts arising from changes in carbon storage, we additionally quantify the radiative forcing of changes in atmospheric CO_2 due to LCC. We employ a empirical methodology proposed by Kirschbaum et al. (2013) and Joos et al. (2013) to calculate changes in atmospheric carbon over time. In contrast to instantaneous biophysical effects, this methodology empirically distributes carbon input/outputs into the four major carbon pools as functions of time. We calculate the change in carbon (ΔC) following LCC per pixel using Eq. (2).

$$C_a = [f_1 + f_2\ exp(\frac{-t}{\tau_2}) + f_3\ exp(\frac{-t}{\tau_3}) + f_4\ exp(\frac{-t}{\tau_4})]\Delta C \quad (2)$$

where $f_1 \ldots f_4$ *and* $\tau_2 \ldots \tau_4$ are the critical constants as displayed by Supplementary Table 1, t are the years since LCC and ΔC in $[tC]$ is the total carbon addition (sum of all gridcells) or removal to/from the atmosphere.

Next, we calculate the radiative forcing from the change in atmospheric carbon as $R_c = 5.35\ ln(1 + (\frac{\Delta C_{atm}}{C}))$ (Myhre et al., 1998) and finally acquire a global $\Delta T_{s(bch)}$ value by multiplying R_c with a climate sensitivity parameter λ as $\Delta T_{s(bch)} = \lambda R_c$ (Forster et al., 2007). To understand the local impacts of the biochemical effect and to facilitate comparison with the biophysical model, we apply a pattern-scaling approach (Tebaldi and Arblaster, 2014). This method determines the spatial response of local temperature changes ($\Delta T_{s(bch)}$) based on the regression of local temperature anomalies on a global temperature anomaly. The spatial pattern is assumed to remain consistent across different global temperature increments, as derived from the ensemble mean of 41 CMIP5 models. These data were bilinearly interpolated to a $0.5° \times 0.5°$ grid to match the resolution of the land-cover input maps, and then scaled by the global $\Delta T_{s(bch)}$ specific to each scenario (Lynch et al., 2017). Some CMIP5 models include land-cover change, meaning the derived spatial patterns may reflect a sensitivity to biophysical effects in addition to biochemical effects. While this is an inherent feature of the source data, the pattern-scaling approach assumes that all local changes are proportional to the global temperature response, which is solely driven by CO_2 radiative forcing. As we define the net effect as the sum of independently assessed biophysical and biochemical effects, we neglect these interactions between biophysical and biochemical effects. From CMIP5 simulations, Quesada et al. (2018) suggested that such synergistic effects are approximately one order of magnitude smaller than the direct effects.

2.2. General model setup and scenarios

Our model is able to calculate biophysical and biochemical temperature impacts from any two given land-cover input arrays. As a proof-of-concept, we focus on three idealized scenarios and corresponding results of the semi-empirical model: (1) Global deforestation, (2) Maximum Forested World and (3) Historical (1850–2005) LCC (c.f. details in Supplementary material Section 1). As the model only simulates local effects (that is, all pixels are treated independently), stylized scenarios (1) & (2) were designed to understand the impacts of LCC at different locations while (3) serves as a baseline scenario to test the model's ability to simulate historical impacts of LCC.

2.3. Datasets

We use a historical land-cover reconstruction by Ramankutty and Foley (1999) provided in $0.5° \times 0.5°$ spatial resolution and annual temporal resolution (Meiyappan and Jain, 2012). The data set provides percentages of 28 different land-cover classes for each grid cell. Due to the simplistic nature of our model and the stylized scenarios, we neglect mixed land-cover and use the provided dominant type land-cover which is reduced to 17 land-cover classes (Details in Supplementary material Section 1) and assume each grid cell to be the most dominant land-cover type. For all three scenario designs, we use the RF (Ramankutty and Foley, 1999) basemap of the year 1850 as initial land-cover and modified it for scenario (1) & (2) or used the 2005 map in case of scenario (3). For the interpretation of the results, the dataset was categorized into three sub-regions: boreal (90°N–60°N and 90°S–60°S), temperate (60°N–30°N and 60°S–30°S), and tropical (30°N–30°S) latitudinal segments.

To solve Eq. (1) and the biochemical model (Eq. (2)), we use a variety of input datasets which are listed in Suppl. Table 2. All datasets with different native spatial resolution are bilinearly interpolated to a $0.5° \times 0.5°$ grid based on the land-cover data. Except for the above-ground carbon data (annual input data), we seasonally averaged these data (DJF, JJA, MAM, SON) to represent seasonality in the modeled parameters. Next, we calculate annual averages from these seasonal data as input for the model runs presented here. In addition to the datasets shown in Supplementary Table 2, both the biophysical model (Eq. (1)) and the biochemical model (c.f. Eq. (2)) require data representing the changes in albedo, surface emissivity, Bowen ratio, aerodynamic resistance and above-ground carbon ($\Delta\alpha$, $\Delta\epsilon$, $\Delta\beta$, Δr_a, ΔC). We designed and explored two different methods to allow for a variety of use cases. The first method, named ATT (**ATT**ached from lookup-table) hereafter, is based on a look-up table approach where empirical values are used to create two arrays (before and after LCC) while the difference of these arrays represents the final input into the model. For $\Delta\alpha$, we additionally incorporated the average snow duration per grid cell to account for the increase in albedo during periods with snow cover. The advantage of this method is that users can easily change values in the look-up tables to perform stylized experiments (e.g. deforestation, albedo-optimized crops etc.). The look-up table approach is only realized for albedo and Bowen Ratio, as we expect aerodynamic resistance to be more heterogeneous within one land-cover class due to its coupling with atmospheric variables. The second method, named MPLC (**M**ean **P**er **L**and **C**over) hereafter, uses the input data (see Supplementary Table 2) and calculates the arrays for each parameter corresponding to a given land cover through the average value across this land cover type (see Supplementary Section 6 for variability in between the land cover types). From these values, arrays of the parameters are created for each land cover map (1850 and 2010 or before/after de-/reforestation,

respectively) and finally subtracted. Changes in surface emissivity ($\Delta\epsilon$) are derived from $\Delta\alpha$ as depicted in Section 2.1. Both methods are described in detail including calculation schemes in Suppl. material Section 5. As the input data had unrealistically high values of r_a for some grid cells (mainly due to artifacts along the coasts caused by re-gridding), we removed all grid cells with $r_a > 150\ sm^{-1}$ from further analysis. Conceptually, the Bowen-Ratio approach is not applicable when latent heat flux is absent (or minimal). We therefore substituted β^2 in the denominator of Eq. (1) by the maximum value of the two modeled β before and after the LCC scenario, thus avoiding unrealistic values of $\Delta T_{s(\beta)}$.

For the simulations presented here, we set the model as follows. To realistically account for the time-dependent effect of the biochemical model, we use the corresponding 155 years (1850–2005) for the historical LCC and employ a hypothetical timestep of 100 years for the two stylized scenarios. In all three scenarios, we assume a climate sensitivity of ($\lambda = 0.8\ \mathrm{Wm^{-2}K^{-1}}$) (Knutti et al., 2017). $\Delta\alpha$ is modeled by using the ATT method while all other parameters ($\Delta\beta$, Δr_a, ΔC) are parameterized by the MPLC method.

3. Results

3.1. Stylized global deforestation experiment

In this scenario, the replacement of forest with short vegetation result in a global direct biophysical warming of $\Delta T_{s(bph)} = 1.22 \pm 0.06$ K (mean & 5-pixel dependent student t-test) of which 1.45 ± 0.08 K can be attributed to changes in aerodynamic resistance $\Delta T_{s(r_a)}$, 0.48 ± 0.02 K to the contribution of changes in Bowen ratio $\Delta T_{s(\beta)}$ and modest cooling of -0.71 ± 0.03 K due to changes in albedo $\Delta T_{s(\alpha)}$(Fig. 1). This albedo cooling is more pronounced in boreal and temperate areas than in tropical areas. The spatial pattern of $\Delta T_{s(r_a)}$ is similar to the $\Delta T_{s(\alpha)}$ but with an opposite sign. Accordingly, $\Delta T_{s(bph)}$ responses to deforestation are higher for boreal than for tropical or temperate latitudes.

Overall, non-radiative effects, the sum of effects due to changes in r_a and β ($\Delta T_{s(r_a,\beta)}$), are about 2.6 times larger in magnitude compared to radiative effects ($\Delta T_{s(\alpha)}$). The contribution of $\Delta T_{s(\beta)}$ is an overall warming, which is concentrated over the tropics (Fig. 1g) but mostly of lower magnitude than the contribution of $\Delta T_{s(r_a)}$ (compare Fig. 1b & c). Regarding the net biophysical effects, the $\Delta T_{s(\alpha)}$ cooling is outweighed by the non-radiative contributions almost exclusively. Exceptions are eastern Siberia with its Larch-dominated forests, where $\Delta T_{s(\alpha)}$ cooling together with the slight cooling due to $\Delta T_{s(\beta)}$ can offset the effect of $\Delta T_{s(r_a)}$. In small parts of Alaska, $\Delta T_{s(\alpha)}$ alone offsets the warming effect of $\Delta T_{s(r_a)}$. Particularly large changes occur around 60 °N ($\Delta T_{s(bph)} \approx 3$ K) due to the strong contribution of $\Delta T_{s(r_a)}$ (Fig. 1g). Furthermore, strong impacts are related to tropical deforestation (~ between 10 °N and 30 °N), where effects of both $\Delta T_{s(r_a)}$ and $\Delta T_{s(\alpha)}$ are weaker, but $\Delta T_{s(\beta)}$ has a strong effect ($\Delta T_{s(bph)} \approx 3$ K). Around the equator, all three biophysical contributions cause large changes with the sum of the warming by $\Delta T_{s(\beta)}$ and $\Delta T_{s(r_a)}$ offsetting the cooling of $\Delta T_{s(\alpha)}$ ($\Delta T_{s(bph)} \approx 4$ K). Finally, these warming effects are amplified by the biochemical effect ($\Delta T_{s(bch)} = 0.50$) with 48 ppm of additional atmospheric CO_2 after 100 years.

3.2. Stylized maximum forested world experiment

The ΔT_s response of the Maximum Forested World scenario shows contrasting patterns to the deforestation scenario with a biophysical cooling of -1.95 ± 0.08 K. Although aerodynamic resistance changes remain the dominant contribution in general ($\Delta T_{s(r_a)} = -1.9 \pm 0.08$ K), locally the impacts of changes in the Bowen ratio ($\Delta T_{s(\beta)} = -1.14 \pm 0.04$ K) show strong responses in tropical latitudes (around 5–25 °N in Fig. 2g) with relatively higher importance than in the deforestation scenario (Fig. 1g). Albedo-related warming ($\Delta T_{s(\alpha)} = 1.08 \pm 0.04$ K) dampens the cooling through both non-radiative terms while a calculated uptake of 78 ppm of CO_2 translates into a biochemical cooling of −0.96 K. In contrast to the deforestation scenario, for which minor cooling was observed in Siberia and Alaska, here there are no grid cells for which the contribution by $\Delta T_{s(\beta)}$ has a warming effect. As shown in Fig. 2a, all grid cells with a contribution of $\Delta T_{s(\alpha)}$ show biophysical warming. The highest values are found in the most northern latitudes and for high altitudes such as the Tibetan plateau and the Himalayas. However, the response to albedo change is not limited to these locations with considerable warming patterns at all latitudes (Fig. 2g). The impacts of $\Delta T_{s(r_a)}$ are a global cooling with the strongest responses in the highest latitudes, western North America, several regions of South America,

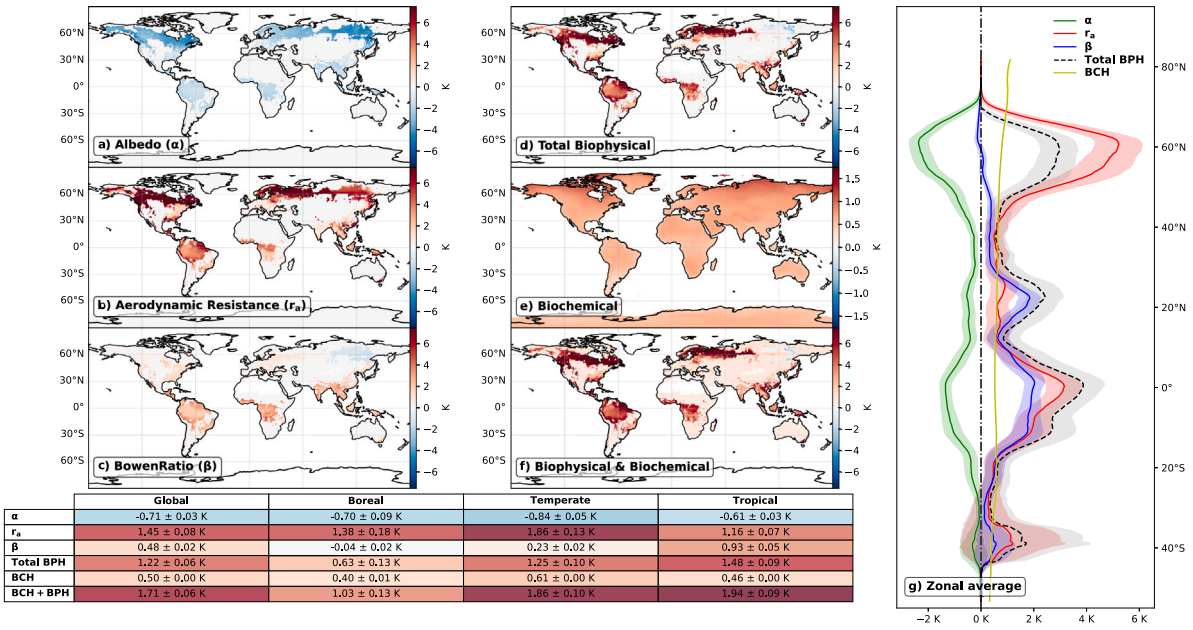

	Global	Boreal	Temperate	Tropical
α	-0.71 ± 0.03 K	-0.70 ± 0.09 K	-0.84 ± 0.05 K	-0.61 ± 0.03 K
r_a	1.45 ± 0.08 K	1.38 ± 0.18 K	1.86 ± 0.13 K	1.16 ± 0.07 K
β	0.48 ± 0.02 K	-0.04 ± 0.02 K	0.23 ± 0.02 K	0.93 ± 0.05 K
Total BPH	1.22 ± 0.06 K	0.63 ± 0.13 K	1.25 ± 0.10 K	1.48 ± 0.09 K
BCH	0.50 ± 0.00 K	0.40 ± 0.01 K	0.61 ± 0.00 K	0.46 ± 0.00 K
BCH + BPH	1.71 ± 0.06 K	1.03 ± 0.13 K	1.86 ± 0.10 K	1.94 ± 0.09 K

Fig. 1. Left and middle panels: Annual local $\Delta T_{s(bph)}$ signal in each grid cell after total deforestation to grass for each contribution: (a), (b) and (c) Albedo, Bowen Ratio and Aerodynamic resistance as in terms (1), (2) and (3) of Eq. (1), (d) total biophysical (BPH) effect (sum of (a), (b) and (c)), (e) biochemical (BCH) effect, (f) Sum of direct BPH and BCH (sum of (d) and (e)). Right panel: Zonally averaged ΔT_s values for BPH (each contribution and sum) and BCH values integrating all continental grid cells of each latitude. Shaded areas indicate the 95% zonal-confidence level (student t-test) of each biophysical effect.

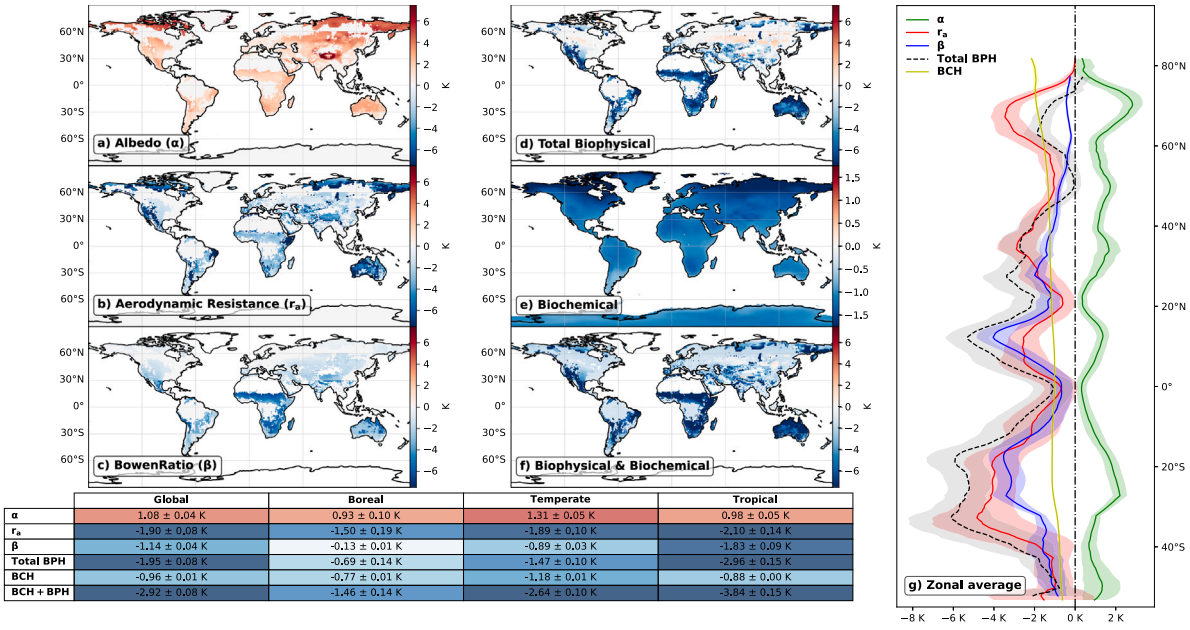

	Global	Boreal	Temperate	Tropical
α	1.08 ± 0.04 K	0.93 ± 0.10 K	1.31 ± 0.05 K	0.98 ± 0.05 K
r_a	-1.90 ± 0.08 K	-1.50 ± 0.19 K	-1.89 ± 0.10 K	-2.10 ± 0.14 K
β	-1.14 ± 0.04 K	-0.13 ± 0.01 K	-0.89 ± 0.03 K	-1.83 ± 0.09 K
Total BPH	-1.95 ± 0.08 K	-0.69 ± 0.14 K	-1.47 ± 0.10 K	-2.96 ± 0.15 K
BCH	-0.96 ± 0.01 K	-0.77 ± 0.01 K	-1.18 ± 0.01 K	-0.88 ± 0.00 K
BCH + BPH	-2.92 ± 0.08 K	-1.46 ± 0.14 K	-2.64 ± 0.10 K	-3.84 ± 0.15 K

Fig. 2. Same as Fig. 1, but for Maximum Forested World experiment.

eastern Africa, Australia, and mountainous regions of Asia (Fig. 2b). As for $\Delta T_{s(r_a)}$, $\Delta T_{s(\beta)}$ is characterized by a global cooling pattern with highest values on the African continent, parts of Australia, the Tibetan plateau, and to a lesser extent on the northern American continents. In high latitudes (above ~50° N), there is little to no contribution by $\Delta T_{s(\beta)}$ (Fig. 2c). For most grid cells, the cooling effects of the non-radiative contributions offset the warming effect of $\Delta T_{s(\alpha)}$. Exceptions are found at the highest latitudes, in some parts of Eurasia, and to a lesser extent in North America (Fig. 2d). There are many strong regional cooling patterns, particularly where both $\Delta T_{s(\beta)}$ and $\Delta T_{s(r_a)}$ contributions are large, as e.g. on the African continent or Australia.

3.3. Historical LCC scenario

The historical LCC experiment results in an average global direct biophysical warming of 0.42 ± 0.07 K (Fig. 3). Here, also, the contribution of $\Delta T_{s(r_a)}$ is dominant estimating the same value as the total effect (0.42 ± 0.07 K), while the magnitude of $\Delta T_{s(\beta)}$ with 0.16 ± 0.02 K is about the same magnitude as $\Delta T_{s(\alpha)}$ which causes a cooling of −0.16 ± 0.03 K, effectively offsetting each other globally. The biochemical model results in an increase in CO_2 of 14 ppm, which corresponds to a biochemical warming of 0.15 K. As the panels in Fig. 3 show, the spatial patterns are more heterogeneous compared to the stylized experiments in Figs. 1 and 2. Impacts of historical LCC in areas that have undergone historical deforestation (e.g. India, parts of the Amazon and central/southern Africa) are broadly similar to patterns found in the deforestation experiment and show the strongest warming patterns (up to ~8 K). Some of the strongest regional cooling patterns are observed in parts of Australia and the western USA (up to ~−8 K, see Fig. 3d). The contribution of $\Delta T_{s(\alpha)}$ is an overall cooling, but with some warming in central Eurasia, Australia and to a smaller extent in western North America, Southern Africa and southern South America (Fig. 3a). The spatial pattern in $\Delta T_{s(r_a)}$ (Fig. 3b) is fairly similar to $\Delta T_{s(\alpha)}$ but opposite in sign and larger in magnitude. For example, $\Delta T_{s(\alpha)}$ reaches ~−4 K in some regions and $\Delta T_{s(r_a)}$ contributes regionally ~6 K, typically associated with deforestation. Although $\Delta T_{s(r_a)}$ and $\Delta T_{s(\alpha)}$ are mostly opposite in sign, there are some regions that reveal ΔT_s sensitivity to changes in roughness with little to no impacts through albedo changes (e.g. eastern Australia, many parts of Eurasia, central North America and Argentina). For the contributions of $\Delta T_{s(\beta)}$, the patterns of biophysical warming are dominating in magnitude over the cooling patterns (compare Fig. 3c).

4. Discussion

In this study, we introduced a physically consistent and computationally efficient tool to quantify the direct biophysical and biochemical effects of LCC on surface temperature. Using three LCC scenarios, we confirm the importance of biophysical effects, particularly the dominant role of non-radiative effects (e.g., changes in aerodynamic resistance and Bowen ratio), which often offset the counteracting cooling effect of albedo increases following deforestation. Regionally, we find substantial local warming of 1.94 K in the tropics, 1.86 K in temperate regions, and 1.03 K in boreal regions following our deforestation scenario.

These results differ from the regional air temperature impacts reported in Chapter 2 of the IPCC Special Report on Climate Change and Land (SRCCL), which identified biophysical changes of 0.61 ± 0.48 K, −0.13 ± 0.22 K and −0.55 ± 0.29 K mean and standard deviation across different model results in the corresponding regions (Jia et al., 2019). While our results indicate an average warming response, the SRCCL reports a dominant cooling response for higher latitudes. It is important to note that air and surface temperature differ and thus cannot be compared directly (e.g. Alkama and Cescatti, 2016; Novick and Katul, 2020). However, at the annual scale, the LCC-induced changes in both variables are known to be correlated (Winckler et al., 2019b), allowing for a qualitative comparison.

The cooling response reported in the SRCCL is related to ESMs including secondary (i.e. indirect) processes such as cloud changes, mesoscale circulation changes, sea ice/sea surface temperature feedbacks, triggered by LCC that further enhance boreal albedo cooling and tend to dominate the global response following stylized scenarios (Alkama and Cescatti, 2016; Quesada et al., 2017; Winckler et al., 2019a; Chen and Dirmeyer, 2020). Studies relying on surface station observations on the other hand (Lee et al., 2011; Zhang et al., 2014) similarly report albedo-driven cooling effects, which is in contrast to our results. This is likely because they capture changes in incoming radiation due to LCC-induced cloud cover changes, particularly important in high latitudes (Chen and Dirmeyer, 2020; Quesada et al., 2017). In contrast, our approach isolates the direct local impacts of LCC, providing a understanding of the underlying surface energy balance components. Our results however do align with studies that isolate direct effects as well. Alkama and Cescatti (2016)

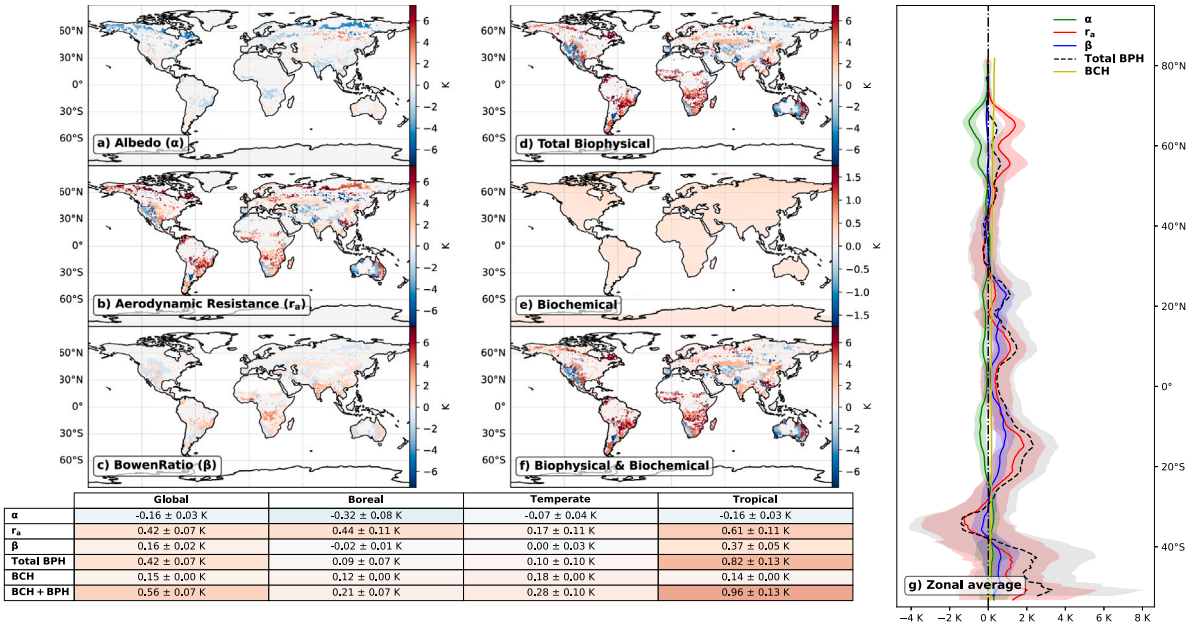

	Global	Boreal	Temperate	Tropical
α	-0.16 ± 0.03 K	-0.32 ± 0.08 K	-0.07 ± 0.04 K	-0.16 ± 0.03 K
r_a	0.42 ± 0.07 K	0.44 ± 0.11 K	0.17 ± 0.11 K	0.61 ± 0.11 K
β	0.16 ± 0.02 K	-0.02 ± 0.01 K	0.00 ± 0.03 K	0.37 ± 0.05 K
Total BPH	0.42 ± 0.07 K	0.09 ± 0.07 K	0.10 ± 0.10 K	0.82 ± 0.13 K
BCH	0.15 ± 0.00 K	0.12 ± 0.00 K	0.18 ± 0.00 K	0.14 ± 0.00 K
BCH + BPH	0.56 ± 0.07 K	0.21 ± 0.07 K	0.28 ± 0.10 K	0.96 ± 0.13 K

Fig. 3. Same as Fig. 1, but for Historical LCC (1850–2005).

for example, quantify the local climate impacts of deforestation by isolating temperature changes attributable to forest cover variations, using a space-for-time substitution approach. They factor out natural climate variability by referencing temperature signals from nearby areas with stable land cover, allowing them to robustly attribute temperature changes to deforestation. Broadly, their findings align with ours, showing overall biophysical warming, including tropical warming and slight but non-significant warming in boreal latitudes. Similarly, offline (i.e. feedback-neglecting) ESM simulations show a comparable pattern of stronger warming following deforestation (e.g. Davin and de Noblet-Ducoudre, 2010; Winckler et al., 2019a; Devaraju et al., 2018) and so do sensitivities found in data-driven assessments (Duveiller et al., 2018).

As expected, the approach emulating ESMs by Nath et al. (2023) efficiently replicates temperature sensitivities as ESM-based studies. In contrast, our method provides mechanistic insights into how and why temperature responds to LCC. These approaches are potentially complementary: our method can identify and quantify individual mechanisms, improving the physical basis of emulator inputs, while a full emulator of an ESM covers large-scale impacts and explore indirect effects not captured by our model.

Taken together, the primary strength of our approach lies in its ability to isolate and quantify the direct biophysical effects of LCC in a simple yet physically consistent manner. This enables a deeper understanding of the fundamental mechanisms driving surface temperature changes, which is particularly important given the uncertainties surrounding biophysical impacts in current ESMs (Jia et al., 2019). Additionally, our method is computationally efficient and flexible, making it a valuable tool for exploring local-to-regional impacts of LCC. On the other hand, our approach is subject to limitations: The linearization of the surface energy balance assumes that there are no interactions between individual components, which may lead to overestimation of ΔT_s, specifically due to the effects of aerodynamic resistance (Rigden and Li, 2017). Another discrepancy stems from the fact that the global averages we calculate are based on continental grid cells only, amplifying the non-radiative contributions relatively larger compared to studies that include oceans. Furthermore, the biochemical effect largely depends on the timescale, rendering the results somewhat arbitrary at least for stylized scenarios. We also acknowledge that, in addition to the uncertainties implicitly included in the input data, a significant number of assumptions are involved. Hence, our analysis is based on the land-cover data from Meiyappan and Jain (2012), available at a 0.5° × 0.5° resolution. To showcase our approach, we used a previously curated dataset where some of the background climate data was only available at a lower resolution than the land cover data. As these data proved reliable in previous assessments, we interpolated them to match the grid of the land-cover data. As a result, finer-scale heterogeneity may not be fully captured. To this end, previous studies have shown strong correlations between adjacent climate model grid cells for temperature (Auffhammer et al., 2013) and among meteorological stations separated by hundreds of kilometers (Gunst, 1995). Similarly, for other variables such as albedo and snow cover, the newer ERA5 reanalysis does not necessarily provide significant improvements over ERA-Interim (e.g. Clelland et al., 2024; Wu et al., 2023). Therefore, we are confident that potential interpolation artifacts do not compromise the validity of our results.

Indeed, despite the model assumptions and input data limitations, our results broadly reproduce the large-scale patterns of surface temperature responses to LCC reported in previous studies, emphasizing the importance of local non-radiative effects. For example, surface roughness and evapotranspiration changes significantly outweigh the albedo effect (e.g. $\Delta T_{s(\beta+r_a)} \approx 1.93$ K vs. $\Delta T_{s(\alpha)} \approx -0.71$ K for the stylized deforestation experiment), consistent with other recent work (Bright et al., 2017; Chen and Dirmeyer, 2016, 2020; Winckler et al., 2019a). While the isolation of the direct local biophysical effects does not realistically capture the full real-world response to large-scale LCC, our approach provides valuable insights into local-scale responses which is the scale where decisions about land use are typically implemented.

Our results thus underscore the importance of considering non-radiative effects in land-based mitigation strategies, particularly in tropical regions where they dominate the surface temperature response. Specifically, we find that accounting for biophysical effects in the tropics, triple the cooling impact of afforestation (−2.92 K; Table in Fig. 2) due to the sole biochemical effect of CO_2 sequestration (0.96 K). As previously discussed, the multiplier factor is likely lower in reality because of the counteracting indirect effect related to lower surface albedo in response to afforestation. However, this remains a crucial message: biophysical effects are roughly the same magnitude (or more) in mitigating climate change as biochemical effects concerning afforestation projects. Tropical afforestation is therefore particularly

justified from a climate change perspective as also suggested by others (Perugini et al., 2017; Jia et al., 2019; Windisch et al., 2022). We also find that afforestation (or reforestation) has a greater impact on the magnitude of changes in temperature than deforestation. For instance, in the Tropics, the magnitude is doubled: biophysical and biochemical effects due to deforestation are respectively, 1.48 K and 0.46 K (Fig. 1), while −2.96 K and −0.88 K in response to afforestation (Fig. 2). While here this is related to our stylized LCC design, Su et al. (2023) showed that the temperature response to tree-cover change is indeed not linear between forest gain and loss. In extra-tropical latitudes, the picture is more nuanced. While boreal regions currently benefit from the snow-masking effect (Betts, 2000), its significance is expected to decline with decreasing snow-cover in a warming climate (Pitman et al., 2011; Pongratz et al., 2021). This further emphasizes the need for regionally tailored strategies when considering the net climate impacts of LCC. Finally, in mere terms of mitigation potential, afforestation or reforestation projects can substantially reduce global warming due to anthropogenic greenhouse gas emissions.

5. Conclusions

Based on key assumptions, Earth Observations and a linearization of the surface energy balance, we present a conceptual model to estimate direct, local and zonal temperature changes due to change in land-cover, disentangling the key biophysical and biochemical mechanisms. We find several key results: (i) the semi-empirical model reproduces zonal temperature changes and coherent biophysical contributions, (ii) local biophysical effects are of similar or greater magnitude as biochemical effects, (iii) afforestation leads to a greater cooling in magnitude than the warming due to deforestation particularly in the Tropics, (iv) non-radiative effects dominate the local surface temperature response to land-cover change. Despite inherent simplifications and uncertainties, the results generally are satisfactory and agree with other recent studies on direct biophysical effects. The great flexibility and the fast calculation time (< 1 s on a normal desktop machine) allow to test many large-scale land-cover policy scenarios and test different values of $\Delta\alpha$, $\Delta\beta$ and Δr_a to assess the robustness and sensitivity of the biophysical effects on surface temperature. Similar approaches could integrate and estimate the impacts of land-use effects (e.g. irrigation), albedo control (e.g. brighter crops, white roofs) or more sophisticated scenarios (e.g. regional deforestation, doubling CO_2 impacts), disentangling the different contributions from relevant parameters.

Due to the reasonable accuracy and the possibility to perform sensitivity experiments to land-cover and their associated parameters easily, our approach is also valuable for informing scientific discussions and educational purposes to understand the underlying physical processes of land-cover changes.

6. Open research

Data sets used are publicly available and can be acquired through the URLs in Supplementary Table 2. A Jupyter Notebook to execute the analysis in the can be run via https://mybinder.org/v2/gh/lohae/LCC_Ts_Emulator/HEAD, is hosted at https://github.com/lohae/LCC_Ts_Emulator and is preserved at https://zenodo.org/doi/10.5281/zenodo.7506358.

CRediT authorship contribution statement

Lorenz Hänchen: Writing – original draft, Visualization, Software, Methodology, Investigation, Formal analysis, Data curation. **Benjamin Quesada:** Writing – review & editing, Validation, Supervision, Methodology, Investigation, Formal analysis, Data curation, Conceptualization. **Almut Arneth:** Writing – review & editing, Supervision, Resources, Project administration, Funding acquisition, Conceptualization.

Declaration of competing interest

The authors declare that they have no known competing financial interests or personal relationships that could have appeared to influence the work reported in this paper.

Acknowledgments

This work was funded by EU-FP7 LUC4C project (603542). We thank the providers of data sets used here (c.f. Suppl. Table 2) and the providers of the python packages xarray, numpy, matplotlib & cartopy and their dependencies. Special thanks to Uwe Schulzweida for the climate data operators (CDO) which we used during the data preparation, Martin Jung for providing us with the sensible and latent heat flux data.

Supplementary material

Supplementary material related to this article can be found online at https://doi.org/10.1016/j.jenvman.2025.124741.

References

Alkama, R., Cescatti, A., 2016. Climate change: Biophysical climate impacts of recent changes in global forest cover. Science 351 (6273), 600–604. http://dx.doi.org/10.1126/science.aac8083.

Arneth, A., Sitch, S., Pongratz, J., Stocker, B.D., Ciais, P., Poulter, B., Bayer, A.D., Bondeau, A., Calle, L., Chini, L.P., Gasser, T., Fader, M., Friedlingstein, P., Kato, E., Li, W., Lindeskog, M., Nabel, J.E., Pugh, T.A., Robertson, E., Viovy, N., Yue, C., Zaehle, S., 2017. Historical carbon dioxide emissions caused by land-use changes are possibly larger than assumed. Nat. Geosci. 10 (2), 79–84. http://dx.doi.org/10.1038/ngeo2882.

Asselin, O., Leduc, M., Paquin, D., Di Luca, A., Winger, K., Bukovsky, M., Music, B., Giguère, M., 2022. On the intercontinental transferability of regional climate model response to severe forestation. Climate 10 (10), 138. http://dx.doi.org/10.3390/cli10100138.

Auffhammer, M., Hsiang, S.M., Schlenker, W., Sobel, A., 2013. Using weather data and climate model output in economic analyses of climate change. Rev. Environ. Econ. Policy 7 (2), 181–198. http://dx.doi.org/10.1093/reep/ret016.

Bala, G., Caldeira, K., Wickett, M., Phillips, T.J., Lobell, D.B., Delire, C., Mirin, A., 2007. Combined climate and carbon-cycle effects of large-scale deforestation. Proc. Natl. Acad. Sci. USA 104 (16), 6550–6555. http://dx.doi.org/10.1073/pnas.0608998104.

Baldocchi, D., Ma, S., 2013. How will land use affect air temperature in the surface boundary layer? Lessons learned from a comparative study on the energy balance of an oak savanna and annual grassland in California, USA. Tellus B: Chem. Phys. Meteorol. 65 (1), 19994. http://dx.doi.org/10.3402/tellusb.v65i0.19994.

Bathiany, S., Claussen, M., Brovkin, V., Raddatz, T., Gayler, V., 2010. Combined biogeophysical and biogeochemical effects of large-scale forest cover changes in the MPI earth system model. Biogeosciences 7 (5), 1383–1399. http://dx.doi.org/10.5194/bg-7-1383-2010.

Betts, R.A., 2000. Offset of the potential carbon sink from boreal forestation by decreases in surface albedo. Nature 408 (6809), 187–190. http://dx.doi.org/10.1038/35041545.

Betts, R.A., 2011. Climate science: Afforestation cools more or less. Nat. Geosci. 4 (8), 504–505. http://dx.doi.org/10.1038/ngeo1223.

Boisier, J.P., De Noblet-Ducoudré, N., Pitman, A.J., Cruz, F.T., Delire, C., Van Den Hurk, B.J., Van Der Molen, M.K., Mller, C., Voldoire, A., 2012. Attributing the impacts of land-cover changes in temperate regions on surface temperature and heat fluxes to specific causes: Results from the first LUCID set of simulations. J. Geophys. Res. Atmospheres 117 (12), http://dx.doi.org/10.1029/2011JD017106.

Bonan, G.B., 2008. Forests and climate change: Forcings, feedbacks, and the climate benefits of forests. Science 320 (5882), 1444–1449. http://dx.doi.org/10.1126/science.1155121.

Bonan, G.B., Pollard, D., Thompson, S.L., 1992. Effects of boreal forest vegetation on global climate. Nature 359 (6397), 716–718. http://dx.doi.org/10.1038/359716a0.

Boysen, L.R., Brovkin, V., Pongratz, J., Lawrence, D.M., Lawrence, P., Vuichard, N., Peylin, P., Liddicoat, S., Hajima, T., Zhang, Y., Rocher, M., Delire, C., Séférian, R., Arora, V.K., Nieradzik, L., Anthoni, P., Thiery, W., Laguë, M.M., Lawrence, D., Lo, M.H., 2020. Global climate response to idealized deforestation in CMIP6 models. Biogeosciences 17 (22), 5615–5638. http://dx.doi.org/10.5194/BG-17-5615-2020.

Bright, R.M., Davin, E., O'Halloran, T., Pongratz, J., Zhao, K., Cescatti, A., 2017. Local temperature response to land cover and management change driven by non-radiative processes. Nat. Clim. Chang. 7 (4), 296–302. http://dx.doi.org/10.1038/nclimate3250.

Brovkin, V., Boysen, L., Arora, V.K., Boisier, J.P., Cadule, P., Chini, L., Claussen, M., Friedlingstein, P., Gayler, V., Van den hurk, B.J., Hurtt, G.C., Jones, C.D., Kato, E., De noblet ducoudre, N., Pacifico, F., Pongratz, J., Weiss, M., 2013. Effect of anthropogenic land-use and land-cover changes on climate and land carbon storage in CMIP5 projections for the twenty-first century. J. Clim. 26 (18), 6859–6881. http://dx.doi.org/10.1175/JCLI-D-12-00623.1.

Cao, F., Dan, L., Ma, Z., Gao, T., 2021. The impact of land use and land cover change on regional climate over East Asia during 1980–2010 using a coupled model. Theor. Appl. Climatol. 145 (1), 549–565. http://dx.doi.org/10.1007/s00704-021-03629-6.

Chen, L., Dirmeyer, P.A., 2016. Adapting observationally based metrics of biogeophysical feedbacks from land cover/land use change to climate modeling. Environ. Res. Lett. 11 (3), 34002. http://dx.doi.org/10.1088/1748-9326/11/3/034002.

Chen, L., Dirmeyer, P.A., 2020. Reconciling the disagreement between observed and simulated temperature responses to deforestation. Nat. Commun. 11 (1), 1–10. http://dx.doi.org/10.1038/s41467-019-14017-0.

Clelland, A.A., Marshall, G.J., Baxter, R., 2024. Evaluating the performance of key ERA-Interim, ERA5 and ERA5-Land climate variables across Siberia. Int. J. Climatol. 44 (7), 2318–2342. http://dx.doi.org/10.1002/joc.8456.

Conte, L., Renner, M., Brando, P., Oliveira dos Santos, C., Silvério, D., Kolle, O., Trumbore, S.E., Kleidon, A., 2019. Effects of tropical deforestation on surface energy balance partitioning in Southeastern Amazonia estimated from maximum convective power. Geophys. Res. Lett. 46 (8), 4396–4403. http://dx.doi.org/10.1029/2018GL081625.

Davin, E.L., de Noblet-Ducoudre, N., 2010. Climatic impact of global-scale Deforestation: Radiative versus nonradiative processes. J. Clim. 23 (1), 97–112. http://dx.doi.org/10.1175/2009JCLI3102.1.

Davin, E.L., de Noblet-Ducoudré, N., Friedlingstein, P., 2007. Impact of land cover change on surface climate: Relevance of the radiative forcing concept. Geophys. Res. Lett. 34 (13), http://dx.doi.org/10.1029/2007GL029678.

Davin, E.L., Rechid, D., Breil, M., Cardoso, R.M., Coppola, E., Hoffmann, P., Jach, L.L., Katragkou, E., de Noblet-Ducoudré, N., Radtke, K., et al., 2020. Biogeophysical impacts of forestation in Europe: first results from the LUCAS (Land Use and Climate Across Scales) regional climate model intercomparison. Earth Syst. Dyn. 11 (1), 183–200. http://dx.doi.org/10.5194/esd-11-183-2020.

De Noblet-Ducoudré, N., Boisier, J.P., Pitman, A., Bonan, G.B., Brovkin, V., Cruz, F., Delire, C., Gayler, V., Van Den Hurk, B.J., Lawrence, P.J., Van Der Molen, M.K., Müller, C., Reick, C.H., Strengers, B.J., Voldoire, A., 2012. Determining robust impacts of land-use-induced land cover changes on surface climate over North America and Eurasia: Results from the first set of LUCID experiments. J. Clim. 25 (9), 3261–3281. http://dx.doi.org/10.1175/JCLI-D-11-00338.1.

Devaraju, N., de Noblet-Ducoudré, N., Quesada, B., Bala, G., 2018. Quantifying the relative importance of direct and indirect biophysical effects of deforestation on surface temperature and teleconnections. J. Clim. 31 (10), 3811–3829. http://dx.doi.org/10.1175/JCLI-D-17-0563.1.

Duveiller, G., Hooker, J., Cescatti, A., 2018. The mark of vegetation change on Earth's surface energy balance. Nat. Commun. 9 (1), 679. http://dx.doi.org/10.1038/s41467-017-02810-8.

Forster, P., Ramaswamy, V., Artaxo, P., Berntsen, T., Betts, R., Fahey, D.W., Haywood, J., Lean, J., Lowe, D.C., Myhre, G., Nganga, J., Prinn, R., Raga, G., Schulz, M., Van Dorland, R., 2007. Changes in atmospheric constituents and in radiative forcing. In: Solomon, S., Qin, D., Manning, M., Chen, Z., Marquis, M., Averyt, K.B., Tignor, M., Miller, H.L. (Eds.), Climate Change 2007: The Physical Science Basis. Contribution of Working Group I To the Fourth Assessment Report of the Intergovernmental Panel on Climate Change, Orgname=Cambridge University Press. Cambridge, United Kingdom and New York, NY, USA, URL: https://www.ipcc.ch/site/assets/uploads/2018/02/ar4-wg1-chapter2-1.pdf.

Forster, P., Storelvmo, T., Armour, K., Collins, W., Dufresne, J.L., Frame, D., Lunt, D.J., Mauritsen, T., Palmer, M.D., Watanabe, M., Wild, M., Zhang, H., 2021. The earth's energy budget, climate feedbacks, and climate sensitivity. In: Masson-Delmotte, V., Zhai, P., Pirani, A., Connors, S.L., Péan, C., Berger, S., Caud, N., Chen, Y., Goldfarb, L., Gomis, M.I., Huang, M., Leitzell, K., Lonnoy, E., Matthews, J.B.R., Maycock, T.K., Waterfield, T., Yelekçi, O., Yu, R., Zhou, B. (Eds.), Climate Change 2021: The Physical Science Basis. Contribution of Working Group I To the Sixth Assessment Report of the Intergovernmental Panel on Climate Change. Cambridge University Press, Cambridge, United Kingdom and New York, NY, USA, URL: https://www.ipcc.ch/report/ar6/wg1/downloads/report/IPCC_AR6_WGI_Chapter_07.pdf.

Fuchs, R., Brown, C., Rounsevell, M., 2020. Europe's Green Deal offshores environmental damage to other nations. Nat. 2021 586: 7831 586 (7831), 671–673. http://dx.doi.org/10.1038/d41586-020-02991-1.

Gerlein-Safdi, C., Keppel-Aleks, G., Wang, F., Frolking, S., Mauzerall, D.L., 2020. Satellite Monitoring of Natural Reforestation Efforts in China's Drylands. One Earth 2 (1), 98–108. http://dx.doi.org/10.1016/j.oneear.2019.12.015.

Gibbs, H.K., Ruesch, A.S., Achard, F., Clayton, M.K., Holmgren, P., Ramankutty, N., Foley, J.A., 2010. Tropical forests were the primary sources of new agricultural land in the 1980s and 1990s. Proc. Natl. Acad. Sci. USA 107 (38), 16732–16737. http://dx.doi.org/10.1073/pnas.0910275107.

Gunst, R.F., 1995. Estimating spatial correlations from spatial-temporal meteorological data. J. Clim. 8 (10), 2454–2470. http://dx.doi.org/10.1175/1520-0442(1995)008<2454:ESCFST>2.0.CO;2.

Hansen, M.C., Potapov, P.V., Moore, R., Hancher, M., Turubanova, S.A., Tyukavina, A., Thau, D., Stehman, S.V., Goetz, S.J., Loveland, T.R., et al., 2013. High-resolution global maps of 21st-century forest cover change. Science 342 (6160), 850–853.

Houghton, R.A., House, J.I., Pongratz, J., Van Der Werf, G.R., Defries, R.S., Hansen, M.C., Le Quéré, C., Ramankutty, N., 2012. Carbon emissions from land use and land-cover change. Biogeosciences 9 (12), 5125–5142. http://dx.doi.org/10.5194/bg-9-5125-2012.

Huang, B., Hu, X., Fuglstad, G.-A., Zhou, X., Zhao, W., Cherubini, F., 2020. Predominant regional biophysical cooling from recent land cover changes in Europe. Nat. Commun. 11 (1), 1066. http://dx.doi.org/10.1038/s41467-020-14890-0.

Jia, G., Shevliakova, E., Artaxo, P., De Noblet-Ducoudré, N., Houghton, R., House, J., Kitajima, K., Lennard, C., Popp, A., Sirin, A., Sukumar, R., Verchot, L., 2019. Land–climate interactions. In: Shukla, P.R., Skea, J., Calvo Buendia, E., Masson-Delmotte, V., Pörtner, H.-O., Roberts, D.C., Zhai, P., Slade, R., Connors, S., van Diemen, R., Ferrat, M., Haughey, E., Luz, S., Neogi, S., Pathak, M., Petzold, J., Portugal Pereira, J., Vyas, P., Huntley, E., Kissick, K., Belkacemi, M., Malley, J. (Eds.), Climate Change and Land: An IPCC Special Report on Climate Change, Desertification, Land Degradation, Sustainable Land Management, Food Security, and Greenhouse Gas Fluxes in Terrestrial Ecosystems. Cambridge University Press, pp. 131–248. http://dx.doi.org/10.1017/9781009157988.004.

Joos, F., Roth, R., Fuglestvedt, J.S., Peters, G.P., Enting, I.G., Von Bloh, W., Brovkin, V., Burke, E.J., Eby, M., Edwards, N.R., Friedrich, T., Frölicher, T.L., Halloran, P.R., Holden, P.B., Jones, C., Kleinen, T., Mackenzie, F.T., Matsumoto, K., Meinshausen, M., Plattner, G.K., Reisinger, A., Segschneider, J., Shaffer, G., Steinacher, M., Strassmann, K., Tanaka, K., Timmermann, A., Weaver, A.J., 2013. Carbon dioxide and climate impulse response functions for the computation of greenhouse gas metrics: A multi-model analysis. Atmos. Chem. Phys. 13 (5), 2793–2825. http://dx.doi.org/10.5194/acp-13-2793-2013.

Juang, J.Y., Katul, G., Siqueira, M., Stoy, P., Novick, K., 2007. Separating the effects of albedo from eco-physiological changes on surface temperature along a successional chronosequence in the southeastern United States. Geophys. Res. Lett. 34 (21), http://dx.doi.org/10.1029/2007GL031296.

Kirschbaum, M.U., Saggar, S., Tate, K.R., Thakur, K.P., Giltrap, D.L., 2013. Quantifying the climate-change consequences of shifting land use between forest and agriculture. Sci. Total Environ. 465, 314–324. http://dx.doi.org/10.1016/j.scitotenv.2013.01.026.

Knutti, R., Rugenstein, M.A., Hegerl, G.C., 2017. Beyond equilibrium climate sensitivity. Nat. Geosci. 10 (10), 727–736. http://dx.doi.org/10.1038/NGEO3017.

Lambin, E.F., Meyfroidt, P., 2011. Global land use change, economic globalization, and the looming land scarcity. Proc. Natl. Acad. Sci. USA 108 (9), 3465–3472. http://dx.doi.org/10.1073/pnas.1100480108.

Lawrence, D., Coe, M., Walker, W., Verchot, L., Vandecar, K., 2022. The unseen effects of deforestation: biophysical effects on climate. Front. For. Glob. Chang. 5, 49. http://dx.doi.org/10.3389/ffgc.2022.756115.

Le Quéré, C., Andrew, R.M., Canadell, J.G., Sitch, S., Korsbakken, J.I., Peters, G.P., Manning, A.C., Boden, T.A., Tans, P.P., Houghton, R.A., et al., 2016. Global carbon budget 2016 global carbon budget 2016. Earth Syst. Sci. Data 8 (2), 605–649. http://dx.doi.org/10.5194/essd-8-605-2016.

Lee, X., Goulden, M.L., Hollinger, D.Y., Barr, A., Black, T.A., Bohrer, G., Bracho, R., Drake, B., Goldstein, A., Gu, L., Katul, G., Kolb, T., Law, B.E., Margolis, H., Meyers, T., Monson, R., Munger, W., Oren, R., Paw U, K.T., Richardson, A.D., Schmid, H.P., Staebler, R., Wofsy, S., Zhao, L., 2011. Observed increase in local cooling effect of deforestation at higher latitudes. Nature 479 (7373), 384–387. http://dx.doi.org/10.1038/nature10588.

Li, Y., Piao, S., Li, L.Z., Chen, A., Wang, X., Ciais, P., Huang, L., Lian, X., Peng, S., Zeng, Z., Wang, K., Zhou, L., 2018. Divergent hydrological response to large-scale afforestation and vegetation greening in China. Sci. Adv. 4 (5), http://dx.doi.org/10.1126/sciadv.aar4182.

Luyssaert, S., Jammet, M., Stoy, P.C., Estel, S., Pongratz, J., Ceschia, E., Churkina, G., Don, A., Erb, K., Ferlicoq, M., et al., 2014. Land management and land-cover change have impacts of similar magnitude on surface temperature. Nat. Clim. Chang. 4 (5), 389–393. http://dx.doi.org/10.1038/nclimate2196.

Lynch, C., Hartin, C., Bond-Lamberty, B., Kravitz, B., 2017. An open-Access CMIP5 pattern library for temperature and precipitation: Description and methodology. Earth Syst. Sci. Data 9 (1), 281–292. http://dx.doi.org/10.5194/essd-9-281-2017.

Meiyappan, P., Jain, A.K., 2012. Three distinct global estimates of historical land-cover change and land-use conversions for over 200 years. Front. Earth Sci. 6 (2), 122–139. http://dx.doi.org/10.1007/s11707-012-0314-2.

Myhre, G., Highwood, E.J., Shine, K.P., Stordal, F., 1998. New estimates of radiative forcing due to well mixed greenhouse gases. Geophys. Res. Lett. 25 (14), 2715–2718. http://dx.doi.org/10.1029/98GL01908.

Myhre, G., Shindell, D., Bréon, F.-M., Collins, W., Fuglestvedt, J., Huang, J., Koch, D., Lamarque, J.-F., Lee, D., Mendoza, B., Nakajima, T., Robock, A., Stephens, G., Takemura, T., Zhang, H., 2013. Anthropogenic and natural radiative forcing. In: Stocker, T., Qin, D., Plattner, G.-K., Tignor, M., Allen, S., Boschung, J., Nauels, A., Xia, Y., Bex, V., Midgley, P. (Eds.), Climate Change 2013: The Physical Science Basis. Contribution of Working Group I to the Fifth Assessment Report of the Intergovernmental Panel on Climate Change. Cambridge University Press, Cambridge, United Kingdom and New York, NY, USA, pp. 659–740. http://dx.doi.org/10.1017/CBO9781107415324.018.

Nabuurs, G.J., Masera, O., Andrasko, K., Benetiz-Ponce, P., Boer, R., Dutschke, M., Elsiddig, E., Ford-Robertson, J., Frumhoff, P., Karjalainen, T., et al., 2007. Forestry. In: Metz, B., Davidson, O.R., Bosch, P.R., Dave, R., L.A., M. (Eds.), Climate Change 2007: Mitigation. Contribution of Working Group III to the Fourth Assessment Report of the Intergovernmental Panel on Climate Change. Cambridge University Press, Cambridge, United Kingdom and New York, NY, USA, pp. 541–584, https://archive.ipcc.ch/publications_and_data/ar4/wg3/en/ch9.html.

Nath, S., Gudmundsson, L., Schwaab, J., Duveiller, G., De Hertog, S.J., Guo, S., Havermann, F., Luo, F., Manola, I., Pongratz, J., et al., 2023. TIMBER v0.1: a conceptual framework for emulating temperature responses to tree cover change. Geosci. Model. Dev. 16 (14), 4283–4313. http://dx.doi.org/10.5194/gmd-16-4283-2023.

Novick, K.A., Katul, G.G., 2020. The duality of reforestation impacts on surface and air temperature. J. Geophys. Res.: Biogeosci. 125 (4), http://dx.doi.org/10.1029/2019JG005543, e2019JG005543.

Panwar, A., Renner, M., Kleidon, A., 2020. Imprints of evaporative conditions and vegetation type in diurnal temperature variations. Hydrol. Earth Syst. Sci. 24 (10), 4923–4942. http://dx.doi.org/10.5194/hess-24-4923-2020.

Perugini, L., Caporaso, L., Marconi, S., Cescatti, A., Quesada, B., De Noblet-Ducoudré, N., House, J.I., Arneth, A., 2017. Biophysical effects on temperature and precipitation due to land cover change. Environ. Res. Lett. 12 (5), 53002. http://dx.doi.org/10.1088/1748-9326/aa6b3f.

Pielke, R.A., Pitman, A., Niyogi, D., Mahmood, R., McAlpine, C., Hossain, F., Goldewijk, K.K., Nair, U., Betts, R., Fall, S., Reichstein, M., Kabat, P., de Noblet, N., 2011. Land use/land cover changes and climate: Modeling analysis and observational evidence. Wiley Interdiscip. Rev.: Clim. Chang. 2 (6), 828–850. http://dx.doi.org/10.1002/wcc.144.

Pitman, A.J., Avila, F.B., Abramowitz, G., Wang, Y.P., Phipps, S.J., De Noblet-Ducoudré, N., 2011. Importance of background climate in determining impact of land-cover change on regional climate. Nat. Clim. Chang. 1 (9), 472–475. http://dx.doi.org/10.1038/nclimate1294.

Pongratz, J., Schwingshackl, C., Bultan, S., Obermeier, W., Havermann, F., Guo, S., 2021. Land use effects on climate: Current state, recent progress, and emerging topics. Curr. Clim. Chang. Rep. 7 (4), 99–120. http://dx.doi.org/10.1007/S40641-021-00178-Y.

Quesada, B., Arneth, A., De Noblet-Ducoudré, N., 2017. Atmospheric, radiative, and hydrologic effects of future land use and land cover changes: A global and multimodel climate picture. J. Geophys. Res. 122 (10), 5113–5131. http://dx.doi.org/10.1002/2016JD025448.

Quesada, B., Arneth, A., Robertson, E., de Noblet-Ducoudré, N., 2018. Potential strong contribution of future anthropogenic land-use and land-cover change to the terrestrial carbon cycle. Environ. Res. Lett. 13 (6), 064023. http://dx.doi.org/10.1088/1748-9326/aac4c3.

Ramankutty, N., Foley, J.A., 1999. Estimating historical changes in land cover North American croplands from 1850 to 1992. Glob. Ecol. Biogeogr. 8 (5), 381–396. http://dx.doi.org/10.1046/j.1365-2699.1999.00141.x.

Rigden, A.J., Li, D., 2017. Attribution of surface temperature anomalies induced by land use and land cover changes. Geophys. Res. Lett. 44 (13), 6814–6822. http://dx.doi.org/10.1002/2017GL073811.

Su, Y., Zhang, C., Ciais, P., Zeng, Z., Cescatti, A., Shang, J., Chen, J.M., Liu, J., Wang, Y.-P., Yuan, W., et al., 2023. Asymmetric influence of forest cover gain and loss on land surface temperature. Nat. Clim. Chang. 13 (8), 823–831. http://dx.doi.org/10.1038/s41558-023-01757-7.

Sy, S., Quesada, B., 2020. Anthropogenic land cover change impact on climate extremes during the 21st century. Environ. Res. Lett. 15 (3), 034002. http://dx.doi.org/10.1088/1748-9326/ab702c.

Tebaldi, C., Arblaster, J.M., 2014. Pattern scaling: Its strengths and limitations, and an update on the latest model simulations. Clim. Change 122 (3), 459–471. http://dx.doi.org/10.1007/S10584-013-1032-9/FIGURES/5.

Winckler, J., Lejeune, Q., Reick, C.H., Pongratz, J., 2019a. Nonlocal effects dominate the global mean surface temperature response to the biogeophysical effects of deforestation. Geophys. Res. Lett. 46 (2), 745–755. http://dx.doi.org/10.1029/2018GL080211.

Winckler, J., Reick, C.H., Luyssaert, S., Cescatti, A., Stoy, P.C., Lejeune, Q., Raddatz, T., Chlond, A., Heidkamp, M., Pongratz, J., 2019b. Different response of surface temperature and air temperature to deforestation in climate models. Earth Syst. Dyn. 10 (3), 473–484. http://dx.doi.org/10.5194/ESD-10-473-2019.

Windisch, M.G., Humpenöder, F., Lejeune, Q., Schleussner, C.-F., Lotze-Campen, H., Popp, A., 2022. Accounting for local temperature effect substantially alters afforestation patterns. Environ. Res. Lett. 17 (2), 024030. http://dx.doi.org/10.1088/1748-9326/ac4f0e.

Wu, H., Xu, X., Luo, T., Yang, Y., Xiong, Z., Wang, Y., 2023. Variation and comparison of cloud cover in MODIS and four reanalysis datasets of ERA-interim, ERA5, MERRA-2 and NCEP. Atmos. Res. 281, 106477. http://dx.doi.org/10.1016/j.atmosres.2022.106477.

Zhang, M., Lee, X., Yu, G., Han, S., Wang, H., Yan, J., Zhang, Y., Li, Y., Ohta, T., Hirano, T., Kim, J., Yoshifuji, N., Wang, W., 2014. Response of surface air temperature to small-scale land clearing across latitudes. Environ. Res. Lett. 9 (3), 34002. http://dx.doi.org/10.1088/1748-9326/9/3/034002.

Zhao, K., Jackson, R.B., 2014. Biophysical forcings of land-use changes from potential forestry activities in North America. Ecol. Monograph. 84 (2), 329–353. http://dx.doi.org/10.1890/12-1705.1.

Further reading

Beringer, J., Chapin, F.S., Thompson, C.C., McGuire, A.D., 2005. Surface energy exchanges along a tundra-forest transition and feedbacks to climate. Agricult. Forest. Meterol. 131 (3–4), 143–161. http://dx.doi.org/10.1016/j.agrformet.2005.05.006.

Compo, G.P., Whitaker, J.S., Sardeshmukh, P.D., Matsui, N., Allan, R.J., Yin, X., Gleason, B.E., Vose, R.S., Rutledge, G., Bessemoulin, P., Bronnimann, S., Brunet, M., Crouthamel, R.I., Grant, A.N., Groisman, P.Y., Jones, P.D., Kruk, M.C., Kruger, A.C., Marshall, G.J., Maugeri, M., Mok, H.Y., Nordli, O., Ross, T.F., Trigo, R.M., Wang, X.L., Woodruff, S.D., Worley, S.J., 2009. NOAA CIRES Twentieth Century Global Reanalysis Version 2. Res. Data Arch. At Natl. Cent. Atmospheric Res. Comput. Inf. Syst. Lab. 10, D6QR4V37, URL: http://dx.doi.org/10.5065/D6QR4V37.

Dee, D.P., Uppala, S.M., Simmons, A.J., Berrisford, P., Poli, P., Kobayashi, S., Andrae, U., Balmaseda, M.A., Balsamo, G., Bauer, P., Bechtold, P., Beljaars, A.C., van de Berg, L., Bidlot, J., Bormann, N., Delsol, C., Dragani, R., Fuentes, M., Geer, A.J., Haimberger, L., Healy, S.B., Hersbach, H., Hólm, E.V., Isaksen, L., Kållberg, P., Köhler, M., Matricardi, M., Mcnally, A.P., Monge-Sanz, B.M., Morcrette, J.J., Park, B.K., Peubey, C., de Rosnay, P., Tavolato, C., Thépaut, J.N., Vitart, F., 2011. The ERA-Interim reanalysis: Configuration and performance of the data assimilation system. Q. J. R. Meteorol. Soc. 137 (656), 553–597. http://dx.doi.org/10.1002/qj.828.

Hänchen, L., Quesada, B., Arneth, A., 2024. Supplementary Jupyter Notebook to Non-radiative effects dominate the local surface temperature response to land-cover change - insights from a semi-empirical model. http://dx.doi.org/10.5281/zenodo.14309419, URL: https://github.com/lohae/LCC_Ts_Emulator.

Jung, M., Reichstein, M., Margolis, H.A., Cescatti, A., Richardson, A.D., Arain, M.A., Arneth, A., Bernhofer, C., Bonal, D., Chen, J., Gianelle, D., Gobron, N., Kiely, G., Kutsch, W., Lasslop, G., Law, B.E., Lindroth, A., Merbold, L., Montagnani, L., Moors, E.J., Papale, D., Sottocornola, M., Vaccari, F., Williams, C., 2011. Global patterns of land-atmosphere fluxes of carbon dioxide, latent heat, and sensible heat derived from eddy covariance, satellite, and meteorological observations. J. Geophys. Res.: Biogeosciences 116 (3), http://dx.doi.org/10.1029/2010JG001566.

Kalnay, E., Kanamitsu, M., Kistler, R., Collins, W., Deaven, D., Gandin, L., Iredell, M., Saha, S., White, G., Woollen, J., et al., 1996. The NCEP/NCAR 40-year reanalysis project. Bull. Am. Meteorol. Soc. 77 (3), 437–471. http://dx.doi.org/10.1175/1520-0477(1996)077%3C0437:TNYRP%3E2.0.CO;2.

Lamptey, B., 2010. An analytical framework for estimating the urban effect on climate. Int. J. Climatol. 30 (1), 72–88. http://dx.doi.org/10.1002/joc.1873.

Liu, Y.Y., Van Dijk, A.I., De Jeu, R.A., Canadell, J.G., McCabe, M.F., Evans, J.P., Wang, G., 2015. Recent reversal in loss of global terrestrial biomass. Nat. Clim. Chang. 5 (5), 470–474. http://dx.doi.org/10.1038/nclimate2581.

Prentice, I.C., Cramer, W., Harrison, S.P., Leemans, R., Monserud, R.A., Solomon, A.M., 1992. A global biome model based on plant physiology and dominance, soil properties and climate. J. Biogeogr. 19 (2), 117–134. http://dx.doi.org/10.2307/2845499.

Rodrigues, T.R., de Paulo, S.R., Novais, J.W.Z., Curado, L.F.A., Nogueira, J.S., de Oliveira, R.G., Lobo, F.d.A., Vourlitis, G.L., 2013. Temporal patterns of energy balance for a Brazilian tropical savanna under contrasting seasonal conditions. Int. J. Atmos. Sci. 2013, 1–9. http://dx.doi.org/10.1155/2013/326010.

Schulzweida, U., 2022. CDO User Guide. http://dx.doi.org/10.5281/zenodo.7112925, Zenodo.

Sertel, E., Robock, A., Ormeci, C., 2010. Impacts of land cover data quality on regional climate simulations. Int. J. Climatol. 30 (13), 1942–1953. http://dx.doi.org/10.1002/joc.2036.

Thompson, C., Beringer, J., Chapin, F.S., McGuire, A.D., 2004. Structural complexity and land-surface energy exchange along a gradient from arctic tundra to boreal forest. J. Veg. Sci. 15 (3), 397–406. http://dx.doi.org/10.1111/j.1654-1103.2004.tb02277.x.

U.S. EPA, 2004. User's Guide for the AERMOD Meteorological Preprocessor (AERMET). Research Triangle Park, NC, Office of Air Quality, p. 252.